CHAPTER 3

Model of free carbon formation when firing an artillery piece

Oleksandr Brunetkin
Pavlo Gultsov
Oleksandr Sidelnykov

Abstract

A phenomenon present in almost every shot, yet rarely addressed or explained in the literature, has been identified. It manifests itself in the muzzle discharge in the form of a certain volume of soot. The Boudouard thermochemical reaction (also referred to in some sources as the Boudouard-Bell reaction carbon monoxide disproportionation), which accounts for soot formation in propellant gases during firing, has been identified. The conditions under which this reaction can occur are discussed. A distinctive feature of this reaction is the formation of a condensed carbon phase during the firing process after gasification of the propellant charge.

Based on the physicochemical processes governing the expansion of propellant gases in the gun barrel, a mathematical model is proposed that makes it possible to estimate the temperature distribution during firing. The initial model is constructed using generally accepted assumptions. The modeling results obtained on its basis can therefore only be regarded as approximate. For this reason, the method relies on simple calculations, making it unnecessary to employ high-performance computing equipment.

A simulation of the temperature distribution of propellant gases along the barrel, between the chamber and the moving projectile, was carried out using a model system similar to the 2A38 artillery system. The possibility of varying the extent of the Boudouard-Bell reaction zone (the soot formation zone) depending on the initial parameters is demonstrated. The use of both fresh and degraded propellant charges was modeled. Full and reduced charges were considered. The simulation results reveal the cause of possible initiation of a secondary muzzle flash, both from the frontal side and from the side of the muzzle brake.

Keywords

Gun, propellant gases, temperature distribution, disproportionation reaction, soot, muzzle flash.

 DOI: 10.21303/978-9908-8450-1-2.ch3

3.1 The role of muzzle discharge in assessing the parameters of internal ballistics processes

In many cases, when solving internal ballistics problems, the thermodestruction (thermal (thermochemical) decomposition) process of a propellant charge is considered under the following assumptions:

– a lumped-parameter model of the thermochemical transformation of the propellant charge is used;

– once formed, the composition of the propellant gases (PG) is assumed to remain unchanged ("frozen") throughout the entire firing cycle;

– the temperature and pressure of the propellant gases are treated as time-dependent variables but are assumed to be spatially uniform over the entire length of the bore behind the projectile at any given moment.

These assumptions are restrictive, yet well balanced for the model employed. Such a model makes it possible to identify general trends and the order of magnitude of the parameters governing internal ballistics processes. Subsequently, the obtained values are refined using empirical correction coefficients.

This approach is effective when the composition of the nitrocellulose (NC) propellant is known and specified. However, during storage, propellants undergo changes in composition and energetic characteristics (degradation). In peacetime conditions, this issue is addressed through laboratory monitoring of propellant condition and their disposal when necessary. Under conditions of intensive use (combat conditions), propellants may be supplied from various storage depots or even from different countries with uncontrolled storage conditions. As a result, batches of charges may be encountered, which characteristics would require disposal in peacetime. At the same time, instrumental inspection of such large volumes of propellants, especially under field conditions, is impracticable.

Changes in propellant composition, often uncontrolled, lead to variations in the parameters of internal ballistics processes. This, in turn, results in reduced firing accuracy, the need to expend a greater number of projectiles to engage a target, increased wear of materiel, and decreased combat survivability of a unit due to longer exposure time at firing positions [1].

Muzzle discharge and the subsequent muzzle flash are among the effects accompanying a shot. These phenomena are usually attributed to external ballistics, more precisely to muzzle (transitional) phenomena. In classical ballistics, muzzle discharge is often identified as a transitional region between internal and external ballistics. It can therefore be assumed that its features and characteristics are shaped by internal ballistics processes, representing a manifestation

of the thermodestruction of the propellant and reflecting the specific nature of these processes.

Muzzle discharge and muzzle flash can be recorded by video with minimal expenditure of time and resources under virtually any conditions, including combat. Analysis of their features and characteristics may serve as a basis for analyzing and assessing the parameters of internal ballistics processes and, ultimately, for evaluating the condition of propellant charges.

3.2 Characteristics of the muzzle discharge

Nitrocellulose propellants are generally classified as smokeless powders. Laboratory experiments record only small amounts of condensed-phase products during and after the thermal decomposition of nitrocellulose propellants. In the available literature, the presence of such products is mainly attributed to various additives contained in the propellant formulations. However, frame-by-frame imaging of the firing process (**Fig. 3.1–3.3**) reveals a different picture. In the muzzle discharge, prior to the onset of the muzzle flash, a substantial amount of soot is observed. The presence of soot in the discharge is the result of reactions occurring inside the barrel during the firing process. Nevertheless, a well-substantiated and generally accepted explanation of these reactions is absent from the available literature.

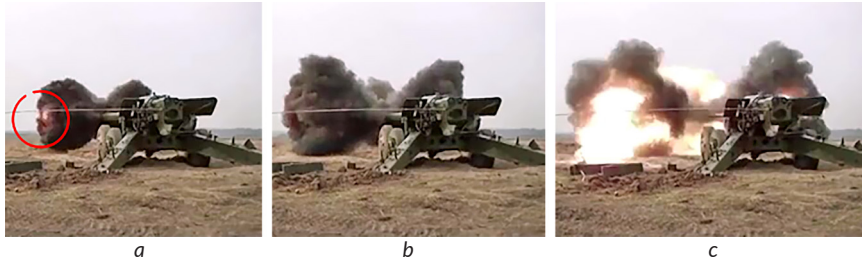

a *b* *c*

Fig. 3.1 Stages in the development of the muzzle discharge of a 152-mm 2A36 gun shot, recorded from ground level: *a* – initial stage characterized by the ejection of soot lobes from the muzzle with the onset of ignition inside one of the lobes; *b* – intermediate stage showing significant expansion of the soot lobes with weak internal combustion traces; *c* – final stage with further enlargement of the discharge cloud and extensive visible flaming within the soot formation

The composition of a propellant and its energetic characteristics can be inferred from the composition of its thermal decomposition products-namely, the propellant

gases (PG). However, even the qualitative composition of PG is reported inconsistently across different sources. Most nitrocellulose (NC) propellants are characterized by a negative oxygen balance. Under these conditions, it remains unclear which compounds are formed in the PG and in what proportions the oxygen contained in the NC propellant participates in their formation.

a *b* *c*

Fig. 3.2 Stages in the development of the muzzle discharge of a 152-mm 2A36 gun shot, recorded from an elevated vantage point: *a* – initial stage showing a three-lobed soot discharge (left, right, and forward lobes) with the onset of ignition inside the lobes; *b* – intermediate stage characterized by full involvement of the discharge cloud in visible flaming; *c* – final stage where the soot clouds are observed at a considerable distance from the muzzle during burnout, while a lighter-colored gaseous jet emerges from the barrel

a *b*

Fig. 3.3 Examples illustrating the presence of soot in the muzzle discharge: *a*, *b* – intermediate combustion phases of soot clouds recorded between the onset of ignition and full involvement of the discharge in flame

Thus, a number of sources, for example [2], assert that PG consists predominantly of gaseous reaction products in the form of vapors of H_2O, CO, CO_2, H_2, and N_2. This description corresponds to the Kistiakowsky-Wilson rule. A negative oxygen balance indeed favors the formation of free hydrogen. However, such an assumption is not supported by the composition of the products of combustion and detonation of nitrated high-energy materials. In particular, studies [3, 4] report the

presence of soot in explosion products. In [5], not only is the presence of soot in the muzzle exhaust documented, but an attempt is also made to quantify it in the course of investigating the muzzle flash. At the same time, the mechanisms responsible for its formation are not discussed.

In [6], a modified Kistiakowsky-Wilson rule is proposed. According to this rule, oxygen from nitro compounds first completely binds hydrogen atoms to form H_2O vapor. It then binds carbon atoms to form CO, and only thereafter does the remaining oxygen further oxidize CO to CO_2. On this basis, the appearance of free carbon in PG in the form of soot can be explained. However, under such a scheme and with a negative oxygen balance, there is insufficient oxygen even to bind all carbon atoms to CO; the formation of H_2 and appreciable amounts of CO_2 is not accounted for.

Thus, the composition of PG corresponds neither to the original nor to the modified Kistiakowsky-Wilson rule, nor to the composition of PG obtained under laboratory conditions. In addition to CO and H_2O vapor, PG contains CO_2, H_2, and as shown in **Fig. 3.1–3.3** – free carbon in the form of soot.

An analysis of **Fig. 3.1–3.3** also makes it possible to identify other features of the muzzle exhaust and muzzle flash and, consequently, potential characteristics of the internal ballistic processes of propellant thermal decomposition:

– in [7], the muzzle flash is attributed to the ignition in air of combustible PG components, namely CO and H_2. The initiating factor is assumed to be the muzzle blast, which causes additional heating of the PG. Given the finite spatial extent of the blast, ignition would be expected to occur over an extended surface. However, the images in **Fig. 3.1**, ***a*** and **Fig. 3.2**, ***a*** demonstrate point-like ignition at the leading front of the exhaust plume, in its central region (outlined in red). At the same time, the photograph in **Fig. 3.3**, ***b*** indicates the possibility of PG ignition on the opposite side of the muzzle exhaust – near the muzzle brake – which cannot be explained by the action of the muzzle blast;

– within the framework of the PG composition discussed above, the intense luminosity of the muzzle flash can be explained by soot combustion. Combustion of gaseous H_2 and CO in air is practically colorless. In **Fig. 3.2**, ***b***, against the bright background of burning soot, a low-contrast gaseous jet can be distinguished (outlined in red). It is located in the leading part of the exhaust plume. A similar jet can also be identified in the trailing part of the muzzle exhaust (**Fig. 3.2**, ***c***, outlined in yellow). The inhomogeneous structure of the muzzle exhaust may be caused by longitudinal nonuniformity in the composition of PG. This, in turn, may indicate a similar nonuniformity in the PG composition along the barrel length at the moment the projectile exits the muzzle.

3.3 Possible causes of the specific features of the muzzle exhaust as a consequence of internal ballistics processes

In the previous section, the following characteristic features of the muzzle exhaust were identified:

– the presence of a significant amount of condensed carbon (soot);

– the possibility of muzzle flash initiation in various regions of the muzzle exhaust;

– heterogeneity of the muzzle exhaust structure with respect to the composition of the PG.

When the muzzle exhaust is considered as a transitional region, its distinctive features should be interpreted as a consequence of internal ballistics processes associated with the thermal decomposition of NC propellant. However, a lumped-parameter model of these processes does not allow the aforementioned features to be adequately explained.

At present, computational resources make it possible to solve internal ballistics problems using distributed-parameter formulations. Increasing model complexity may potentially improve the accuracy and reliability of the results. At the same time, model modification should not be limited solely to increasing computational complexity, but should also incorporate more subtle physical and chemical effects. The following studies may be cited as illustrative examples. Thus, in [8] the solution is obtained within a one-dimensional formulation, whereas in [9] a three-dimensional formulation is employed. In both studies, only the motion of propellant gases inside the barrel is considered. Their composition is assumed to remain constant during the motion. Despite the significantly higher computational complexity of the approach used in [9], the results obtained in both studies are comparable. In another case, the article [10] investigates the muzzle flash process. A model is employed that describes gas-dynamic processes in a two-dimensional formulation, as well as ignition and combustion of propellant gases in atmospheric oxygen. The reversibility of chemical reactions is taken into account, and reaction rates are calculated. It is correctly noted that the characteristics of the muzzle exhaust and muzzle flash depend on the parameters of internal ballistics processes. However, despite the detailed modeling of the exhaust and flash, the internal ballistics processes themselves are treated by neglecting multicomponent effects and chemical reactions. As a result, the possibility of free carbon formation during firing is not considered, nor is its influence on the muzzle flash process taken into account.

In many cases, chemical reactions of NC propellant thermal decomposition during firing are considered from the standpoint of chemical equilibrium. This approach is justified by the high temperatures and pressures at which these processes

occur. However, significant variations of these parameters during the firing process – both in time and along the barrel length at any given moment – may give rise to reversible chemical reactions between the formed components of the propellant gases. For example, the computational results presented in [1] demonstrate that, at certain moments in time, temperature differences along the propellant gas column may reach 500 K or more.

The equilibrium composition calculation method makes it possible to determine the relative proportions of the components constituting the propellant gases and their temperature, but not the actual list of species itself. The set of possible reaction products is specified prior to the calculation. Thus, in [11], results of propellant gas composition calculations based on three different models are presented. Each model assumes a different composition of propellant gases. Some components are common to all models; however, their calculated quantities for the same propellant may differ by several times depending on the model used. Among the considered approaches, the Kamlet-Jacobs model included free carbon and carbon dioxide (CO_2) in the propellant gas composition, but did not account for the presence of carbon monoxide (CO). As a result, calculations based on this model for various propellant formulations yielded free carbon contents of 20–30%, which clearly contradicts practical ballistic applications of propellant mixtures. Moreover, the calculated combustion products do not contain hydrogen or other combustible species, which also contradicts the flame observed when combustion products exit the barrel. These results indicate the necessity of an adequate selection of the propellant gas composition to enable correct calculation of their quantities.

The article [12] presents results of equilibrium composition calculations for the reaction products of methane (CH_4) with oxygen (O_2) under oxygen-deficient conditions (oxidizer excess coefficient $\alpha = 0.6$, corresponding to a negative oxygen balance). The list of possible reaction products included H_2O, H_2, CO_2, CO, and free carbon (C_{crb}). The equilibrium composition of reaction products corresponding to temperatures ranging from the combustion temperature (~1780 K) down to 500 K was analyzed. A characteristic feature is noted in [12]. At the combustion temperature, free carbon is not detected. However, as the temperature decreases, starting from approximately 1300–1200 K, the possibility of free carbon formation is shown. Simultaneously, the amount of CO decreases while the amount of CO_2 increases. Beginning at temperatures of approximately 700 K, the calculated results no longer indicate the presence of CO. Under normal ambient conditions, such behavior is not observed. A mixture of methane (CH_4) and oxygen (O_2) under normal conditions remains stable in the absence of external influences, and free

carbon is not formed. This is explained by the extremely low reaction rate, despite the thermodynamic possibility of the reaction.

A chemical reaction exhibiting similar characteristics is well known. This is the Boudouard-Bell reaction, representing the disproportionation of carbon monoxide (CO) into free carbon

$$2 \cdot CO \leftrightarrow C\downarrow + CO_2 + Q. \tag{3.1}$$

This reaction is characterized by reversibility. At elevated temperatures up to approximately 1300 K, the equilibrium is almost completely shifted toward CO formation. Nevertheless, the reverse reaction remains exothermic. At the same time, equilibrium calculations indicate the formation of a certain amount of free carbon, which is associated with the endergonic nature of CO disproportionation. At temperatures of about 400 K, the thermodynamic equilibrium of the Boudouard-Bell reaction is shifted toward the formation of CO_2 and C. However, under normal or near-normal conditions, CO remains stable due to the low rate of the disproportionation reaction.

During firing, by the moment the projectile exits the barrel, the temperature of the propellant gases decreases to values of approximately 1000 K, corresponding to a shift of the thermodynamic equilibrium of the disproportionation reaction toward the formation of condensed carbon. At the same time, a high pressure of the propellant gases is maintained, which may reach approximately 50 MPa. In accordance with Le Chatelier's principle, high pressure favors a shift of the equilibrium toward the formation of a condensed phase. The disproportionation reaction of CO is of second order. In this case, at identical propellant-gas temperatures, the rate of formation of condensed carbon in the barrel system, compared with laboratory conditions (0.1 MPa), increases by a factor of about $(50/0.1)^2$, i.e., approximately 250,000. This estimate should be regarded as an order-of-magnitude illustration rather than a detailed kinetic description.

It is necessary to consider the possible influence of the process described by reaction (3.1) on changes in the pressure of the propellant gases in the barrel channel as the projectile moves. After completion of the thermodestruction of the propellant charge, the barrel volume behind the projectile continues to increase as it travels, while the amount of propellant gas does not increase. This stage is characterized by an accelerated decrease in propellant-gas pressure. However, under these conditions, prerequisites arise for reaction (3.1) to proceed. Its result is a twofold reduction in the volume of the reacting fraction of the propellant gases, which may locally affect pressure evolution.

3.4 Simplified one-dimensional model of internal ballistics processes

3.4.1 Composition of propellant gases

The structure of the muzzle blast and muzzle flash makes it possible to assess the nature of the distribution of PG parameters along the barrel length at the moment the projectile exits the muzzle. Accordingly, the current composition and energy characteristics of the propellant charge can be estimated from the PG parameters. Such an assessment may be carried out using the library-based method described in [12, 13]. A distinctive feature of this method is the high speed of evaluating the state of the propellant charge. However, this requires the prior creation of a database that reflects the possible values of PG parameters as functions of varying propellant charge compositions and energy characteristics. This, in turn, necessitates solving the internal ballistics problem a very large number of times (hundreds of millions or more). In doing so, the PG parameters along the barrel length must be obtained in a distributed form. Modern computational resources make it possible to perform such calculations within a reasonable time frame. Nevertheless, to adequately represent the PG parameter values, the employed model should be as simple as possible.

The development of such a model is a multistage process involving an assessment of the assumptions adopted at each stage, with a gradual increase in model complexity up to the required level. At the initial stage, it is necessary to evaluate the feasibility of adequately reproducing the character of variation of PG parameters for the chosen overall model structure and computational strategy under the most permissive assumptions.

To assess the possible equilibrium composition of propellant gases at different temperatures, calculations were performed for a propellant charge, which composition is given in [14] and presented in **Table 3.1**.

Table 3.1 Initial composition of the NC propellant charge

Component	Substance	%	Molecular formula
Energetic base	Nitrocellulose	96.0	$C_6H_{7.7}N_{2.3}O_{9.6}$
Plasticizer	Ethanol	0.5	C_2H_6O
	Diethyl ether	0.5	$C_4H_{10}O$
Chemical stability stabilizer	Diphenylamine	1.0	$C_{12}H_{11}N$
Impurity substances	Water (moisture)	2.0	H_2O

Based on these data, the gross formula (molecular formula) of the propellant charge was calculated. The formula is expressed relative to a single carbon atom

$$C_1H_{1.44}N_{0.37}O_{1.57}. \tag{3.2}$$

The determination of the propellant gases' composition is based on solving a system of equations that includes the law of mass action, the law of conservation of matter, and Dalton's law. The enthalpy of formation is also used for both the propellant charge and the components of the propellant gases. The calculation is based on equating the enthalpy of the propellant to the sum of the enthalpies of formation of the propellant gas components, taking their temperature into account.

A distinctive feature of this approach is the specific form of the mass-action equations. The equations are formulated based on the formation reactions of possible propellant gas components from elementary chemical substances [15]. For example:

$$\begin{aligned} &H_2O \rightleftarrows 2\cdot H + O, \\ &CO_2 \rightleftarrows C + 2\cdot O. \end{aligned} \tag{3.3}$$

This form of representation is universal. It allows for the construction of a closed system of equations based on a list of substances that may be present in the mixture. In the established models describing the firing process, the composition of the propellant gases for the propellant charge is determined based on the following list of constituent components

$$H_2O, CO_2, CO, H_2, CH_4, N_2. \tag{3.4}$$

To account for the potential formation of soot, this list is supplemented with an additional component, denoted as C_{crb} (finely dispersed condensed carbon phase). The consideration of carbon in the propellant gases is a specific feature of the model used in the calculations. The method for calculating the thermodynamic parameters of the gaseous mixture in the presence of a condensed phase is given in [15].

The equilibrium composition of the propellant gases at various temperatures is shown in **Fig. 3.4**.

From the calculation results presented in the graphs (**Fig. 3.4**), it follows that the molar concentrations of the propellant gas components remain almost constant over a wide range of temperatures during their expansion in the firing process. However, as noted in [12], at temperatures of 1200–1300 K and below, the quantitative composition of the propellant gas components changes. Condensed

carbon appears. The amounts of not only carbon-containing elements but also all other elements (except for nitrogen, N_2) are altered.

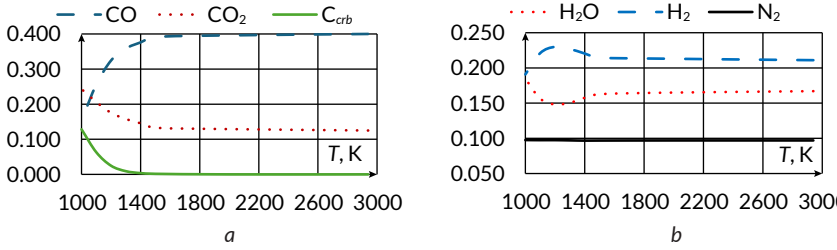

Fig. 3.4 Molar concentrations of propellant gas components as a function of temperature *T*: *a* – carbon-containing components; *b* – carbon-free components

3.4.2 Method for determining propellant gas temperature along the barrel during firing for a distributed-parameter model

At the first stage of developing a model for internal ballistics processes, the values of parameters governing the gas-dynamic processes (pressure and temperature) occurring in the PG along the barrel length at each moment of the shot are averaged. This procedure simplifies the solution. The justification for its use lies in the minor influence of deviations of pressure and temperature from their mean values on the processes under consideration.

For instance, in [16], calculations were performed for a 100 mm, caliber gun with a chamber length of $l_c = 1\,\text{m}$ and a barrel length of $l_d = 5\,\text{m}$. The charge mass varied in the range of 2.5–45 kg. Pressure values were determined at the breech face and at the base of the projectile as it passed the muzzle. For all calculations, the deviation of pressure at the base of the projectile from that at the breech face ranged from 6% to 53%. Deviations of pressure values in different parts of the space behind the moving projectile can affect the accuracy of determining the projectile velocity, but have practically no effect on the composition of the propellant gases. High pressures, regardless of their magnitude, under high PG temperatures imply an equilibrium composition.

Many sources do not use data on the distribution of PG temperature along the barrel during projectile motion. When using models that do not account for the formation of a condensed phase, such information is unnecessary. It is assumed that, during the shot, within the temperature range of the PG, their composition

remains practically unchanged. This is confirmed by the calculation results shown in **Fig. 3.4**. In the range from the combustion temperature (2940 K) to the temperature at which a significant amount of soot begins to form (~1400 K), the PG composition remains nearly constant.

The temporal behavior of the muzzle blast (**Fig. 3.1–3.3**) indicates not only the potential for condensed phase formation but also the non-uniformity of this process along the barrel. To identify the principal possibility of conditions supporting the disproportionation reaction of carbon monoxide, modeling of the PG temperature distribution along the barrel during the shot is necessary. Let's consider the model and the projectile firing process. Let's introduce a set of assumptions corresponding to the first stage of model development:

– the burn rate of the propellant charge depends solely on pressure;

– the propellant volume is neglected;

– PG pressure is uniform (averaged) at all points between the breech face and the base of the projectile;

– during projectile motion, PG movement along the barrel is one-dimensional, with no mixing of newly formed gases with previously generated PG;

– the PG expansion process is adiabatic, with a known adiabatic index;

– backpressure in front of the projectile is neglected;

– energy expenditures for processes other than projectile acceleration are accounted for using a coefficient that increases the projectile mass in calculations (a fictitious projectile mass);

– PG is considered an ideal gas mixture, and covolume effects are neglected.

To account for the PG temperature distribution along the barrel, the mathematical model (MM) must be expressed in partial differential form, which usually requires numerical solution methods. For preliminary assessment of temperature distribution under the adopted assumptions, this approach is impractical. The following approach has been proposed to describe the firing process:

– projectile motion along the barrel is roughly divided into two stages: during propellant combustion and after its completion;

– the propellant burns in discrete portions of equal mass;

– the pressure at which the next portion of the charge burns is assumed constant and equal to the pressure after the previous step of PG expansion. This pressure determines the burning time t_i of the current portion, which also defines the time step for the calculation. The time interval for burning each portion (and thus for the calculation step) is variable depending on the current pressure;

– formation of each new portion of PG mass m_i occurs without affecting the existing PG (e.g., outside the barrel). This step corresponds to the assumption of

neglecting the propellant volume, and thus the change in pre-chamber volume as the propellant burns;

– the newly formed PG portion enters the chamber instantly through its end surface (**Fig. 3.5**). The pressure rises instantaneously, forming a new value p_i, determined by the added PG, as well as the volume ($w_0, w_1, ..., w_{i-1}$) and pressure of the pre-existing PG;

– during the time interval t_i (duration of the current calculation step), PG expansion and projectile acceleration occur (without additional PG input). At the end of this interval, the PG pressure is determined, which is used to calculate the burning time of the next portion of the propellant in the following time step;

– after the propellant is fully burned, the expansion of PG and projectile acceleration are calculated until the projectile exits the barrel.

Fig. 3.5 Diagram of the formation of the incoming gas fraction at the current calculation step

At this stage, the PG temperature distribution along the barrel during the shot is estimated. Average values of certain quantities, corresponding to modern barrel systems, are used in the calculation relationships.

In describing propellant properties, their energetic characteristic is conventionally expressed as their strength *f*. At the same time, the calculation is based on the enthalpy of the NC thermal decomposition reaction. Let's estimate the relationship between these quantities. Assume: the combustion process is isoenthalpic (constant-enthalpy process); the gas-phase process is adiabatic. According to the adopted assumptions

$$I_{sp}^{G} = I_{sp}^{PG} = \frac{\gamma}{\gamma - 1} \cdot f, \tag{3.5}$$

where I_{sp}^{G} – the specific enthalpy of gunpowder; I_{sp}^{PG} – the specific enthalpy of gunpowder gases; γ – the adiabatic index; f – the propellant force.

Let's assume $\gamma = 1.2$, $f = 950$ kJ/kg. In this case $I_{sp}^{G} = 5700$ kJ/kg. Further calculations were performed taking these values into account:

Step 1. From equation (3.5), the temperature of the propellant gas (PG) is determined, and from the equation of state, the amount of propellant charge required to

generate the forcing pressure in the breech chamber is calculated. The magnitude of the forcing pressure, the volume of the breech chamber (excluding the charge volume), and the adiabatic index are specified. Based on the fraction of the charge burned, the enthalpy of the considered PG volume is determined. The remaining mass of the propellant charge is calculated, and the number of calculation steps is selected. The mass of the portion of the charge m_i, which combustion is considered in a single calculation step, is determined. All portions have equal masses. The forcing pressure serves as the initial pressure for the next calculation step and determines the burning rate of the corresponding portion of the propellant charge. This PG volume is hereinafter denoted as w_0 (**Fig. 3.5**).

Step 2. Using the final pressure obtained in Step 1, the burning time t_i of the portion m_i of the propellant charge is determined. A linear burning law $u_1 = u_0 \cdot p$ and a constant burning surface area F are assumed. Accordingly

$$m_i = (u_0 \cdot p) \cdot F \cdot t_i \Rightarrow t_i = \frac{m_i}{(u_0 \cdot F) \cdot p}. \tag{3.6}$$

The method for determining the expression in parentheses is described below.

Step 3. The generated portion of PG is introduced (instantaneously) into the breech chamber without changing its volume. According to the current calculation step number i, this portion of PG is hereinafter denoted as w_i. The enthalpy (I_i^n) of the PG is calculated as the sum of the enthalpy from the end of the previous calculation step and that contributed by the current portion. According to

$$I_i^n = \frac{\gamma}{\gamma - 1} \cdot P_i^n \cdot W_i^n \Rightarrow P_i^n = \frac{\gamma - 1}{\gamma} \cdot \frac{I_i^n}{W_i^n} \tag{3.7}$$

the mixture pressure (P_i^n) at the beginning of the calculation step is determined. Considering the assumption that the PG volumes from the respective calculation steps do not mix, their updated values are calculated.

Step 4. Expansion of the PG and acceleration of the projectile during the current calculation step occur over the time t_i determined in Step 2 and are described by the relation

$$\varphi M \frac{d^2 x}{dt^2} = P \cdot S, \tag{3.8}$$

here M – the projectile mass; φ – the coefficient accounting for the effective mass of the projectile; x – the length of the breech chamber; P – the PG pressure; and S – the cross-sectional area of the barrel.

The value of P is determined from the relation describing the adiabatic expansion of the gas

$$(P_i^n)\cdot(W_i^n)^\gamma=(P_i)\cdot(W_i)^\gamma \Rightarrow P_i=(P_i^n)\cdot\left(\frac{W_i^n}{W_i}\right)^\gamma, \tag{3.9}$$

where P_i^n, W_i^n – the pressure and volume of the breech chamber at the initial moment of the calculation step (corresponding to the values at the end of the previous step); and P_i, W_i – the pressure and volume at the current moment of the calculation.

Taking into account $W_i = S \cdot x_i$ and equation (3.9), expression (3.8) can be rewritten as

$$\frac{d^2x}{dt^2}-\frac{r}{(x)^\gamma}=0, \text{ where } r=\frac{P_i^n\cdot S\cdot(x_i^n)^\gamma}{\varphi\cdot M}, \tag{3.10}$$

here x_i^n – denotes the length of the projectile space at the initial moment of the calculation step.

Let's linearize the second term of equation (3.10) at the point x_i^n. As initial conditions, it is possible to use the values of x_i^n and the projectile velocity v_i^n at the initial moment of the current calculation step (the final velocity from the previous calculation step). Assuming, as before, $\gamma = 1.2$, the solution of (3.10) can be expressed as

$$x(t)=\frac{v^n}{\sqrt{d_1}}\sin(\sqrt{d_1}\cdot t)-\frac{5}{6}x_i^n\cos(\sqrt{d_1}\cdot t)+\frac{11}{6}x_i^n, \text{ where } d_1=\frac{6r}{5x_i^n}. \tag{3.11}$$

By substituting the value of t_i into this expression, the magnitude of the charge-free space x_i^k at the end of the current calculation step is determined, and from the derivative of (3.11)

$$v=x'(t)=v^n\cos(\sqrt{d_1}\cdot t)+\frac{5}{6}x_i^n\sqrt{d_1}\sin(\sqrt{d_1}\cdot t) \tag{3.12}$$

the velocity of the v_i^k projectile at this instant.

Step 5. Under the assumptions adopted, based on the first law of thermodynamics

$$\Delta U = A. \tag{3.13}$$

Taking into account the adiabatic expansion of the propellant gases and, accordingly, $I = \gamma \cdot U$, it follows from equation (3.13) that by the end of the current computational step

$$I_{res} = I_{com} - \gamma \cdot \varphi M \frac{(v_i^k)^2}{2}, \tag{3.14}$$

here ΔU – the change in the internal energy of the propellant gases expended to perform the work A required to accelerate the projectile with the fictitious mass φM; I_{com} – the total enthalpy introduced with the propellant gases into the behind-the-projectile space; and I_{res} – the residual enthalpy at the end of the current computational step after the work of projectile acceleration has been performed. Equation (3.14) may be regarded as a simplified enthalpy-based analogue of the Résal equation. From the relation

$$I_{res} = \frac{\gamma}{\gamma - 1} \cdot P_i^k \cdot W_i^k \Rightarrow P_i^k = \frac{\gamma - 1}{\gamma} \cdot \frac{I_{res}}{W_i^k} \tag{3.15}$$

the pressure of the propellant gases at the end of the calculation step is determined.

Step 6. If, by the beginning of the next calculation step, the entire propellant charge has not been consumed, proceed to Step 2.

Step 7. The calculation is performed in accordance with the method described in Steps 2–5, but without accounting for the inflow of propellant gases into the behind-the-projectile space. The termination time of the calculation is defined as the instant when the projectile reaches the muzzle.

In the course of the calculation, for each propellant-gas element w_i (**Fig. 3.5**), the current temperature can be determined from the equation of state.

3.4.3 Results of modeling the temperature distribution in the barrel region between the chamber and the moving projectile

For the model system (**Table 3.2**) corresponding to the 2A36 gun, the temperature distribution of the propellant gases along the barrel length during the firing process at various time instants was calculated using the method described in the previous section.

The averaged firing characteristics were selected so that the characteristic terminal parameters of the shot were close to the corresponding terminal parameters of the real system (**Table 3.3**).

As a result of the calculations, it was established that when 0.5 kg of propellant charge is burned with the projectile fixed in the chamber, a pressure of approximately $3.06 \cdot 10^7$ Pa is reached, which is close to the adopted value of the forcing pressure. The subsequent combustion process of the remaining portion of the

charge with a mass of 10.5 kg was approximated using a discrete scheme and divided into 35 computational steps with a mass increment of $\Delta m = m_i = 0.3\,\text{kg}$ at each step.

Table 3.2 Firing parameters of the model artillery system

Name	Symbol	Value
Caliber	d, m	0.152
Barrel cross-sectional area	S, m^2	0.0181
Free volume of the propellant chamber (excluding propellant volume)	W_{KC}, m^3	0.0155
Length of the free volume of the propellant chamber	x_{KC}, m	0.85
Projectile mass	M, kg	46
Propellant mass (reduced charge)	m, kg	11
Specific enthalpy of the propellant	I, J/kg	$5.7 \cdot 10^6$
Adiabatic index	γ	1.2

Table 3.3 Characteristic values

Name	Symbol	Value
Forcing pressure	P_p, Pa	$3 \cdot 10^7$
Projectile velocity (for the reduced charge)	V, m/s	775
Projectile velocity at the end of propellant combustion ($\tilde{V} = 0.8 \cdot V$)	$\tilde{V}$, m/s	620

By adjusting the value of the expression in parentheses in formula (3.6), the calculated velocity values $\tilde{V}$ = 633.5 m/s and V = 774.5 m/s were obtained, which are in satisfactory agreement with the reference data presented in **Table 3.3**. In these calculations, the parameter value $u_0 \cdot F = 8.65 \cdot 10^{-8}$ m^3/s was adopted.

Since, during the calculations, the main reference quantities were reproduced with a high degree of proximity to the specified values, it can be reasonably assumed that the resulting calculated temperature distribution of the propellant gases in the space behind the projectile adequately reflects the actual behavior of the process under consideration.

The graphs presented below show the results of the calculations performed on the basis of the data from **Tables 3.2**, **3.3**. **Fig. 3.6** illustrates the variation of propellant gas pressure, while **Fig. 3.7** presents the temperature distribution in the space behind the projectile for different projectile positions corresponding to the scheme shown in **Fig. 3.5**.

It should be noted that the pressure values in **Fig. 3.6** are referred to a point rigidly attached to the base of the projectile, which explains why the initial section

of the curve does not originate at zero. In this case, the abscissa coordinate is determined by the length of the charge chamber, while the ordinate represents the forcing pressure.

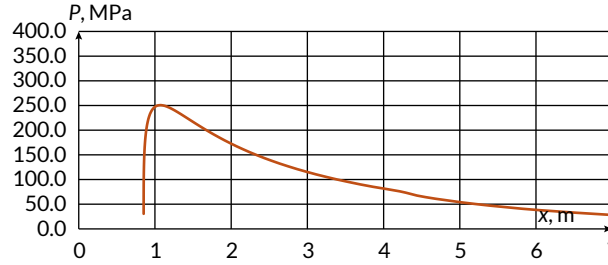

Fig. 3.6 Results of the calculation of the change in the chamber pressure for a reduced charge of fresh propellant in the space behind the projectile
*Source: data from the **Tables 3.2**, **3.3***

In **Fig. 3.7**, the temperature fields are shown for points corresponding to different portions of the propellant gases. All the portions considered have the same mass (0.3 kg in the present calculation); however, due to differences in the instantaneous pressure, their spatial extent in the space behind the projectile is not the same. For this reason, the initial abscissa coordinates of curves 1, 2, and 3 in **Fig. 3.7** do not coincide, which reflects the physical features of the propellant gas distribution during the firing process.

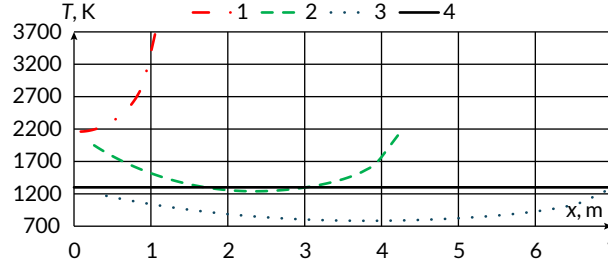

Fig. 3.7 Results of the calculation of changes in the propellant gas temperature for a reduced charge of fresh propellant. Distribution of the propellant gas temperature at various projectile positions: 1 – at the moment of maximum pressure in the space behind the projectile; 2 – at the end of propellant charge combustion; 3 – when the projectile is at the muzzle; 4 – temperature boundary of the Boudouard-Bell reaction
*Source: data from the **Tables 3.2**, **3.3***

Analysis of the results of the performed calculations shows that up to the point of complete combustion of the propellant charge, the conditions for the Boudouard-Bell reaction in the cartridge space are practically absent. This is clearly illustrated by the temperature distributions shown in **Fig. 3.7** (curves 1 and 2): at this stage, the temperature of the propellant gases along the entire length of the cartridge volume predominantly exceeds the lower threshold for the onset of the aforementioned reaction (see also the boundary curve 4 in **Fig. 3.7**). Thus, during the active combustion period of the charge, the formation of a condensed phase in the form of soot is thermodynamically not realized.

A different situation is observed during the subsequent expansion stage of the propellant gases after the completion of charge combustion, which corresponds to the temperature distribution shown in **Fig. 3.7** (curve 3). At this stage, regions are formed in the cartridge space where the temperature drops below the threshold for the carbon monoxide disproportionation reaction, creating conditions for the Boudouard-Bell reaction and, consequently, for the formation of a condensed carbon phase. At the moment the projectile passes the muzzle, the highest temperatures are maintained near the base of the projectile and the base of the chamber.

In the central part of the propellant gas volume, the temperature remains below the threshold value corresponding to the onset of the CO disproportionation reaction for the longest period. It is precisely in this zone that the most intensive formation of the condensed phase is expected, which may have a noticeable effect on the composition of the firing products and the characteristics of the exiting gases.

In order to assess the influence of the degree of degradation of the propellant charge on the magnitude of the main firing parameters, an additional calculation was performed for the propellant with the same gross formula (3.2) but with an 8% reduction in its energy capacity (propellant degradation). Using the adopted specific enthalpy value of I = 5240J/kg and other initial data corresponding to **Tables 3.2**, **3.3**, the calculated dependencies presented in **Fig. 3.8**, **3.9** were obtained. For convenience of comparison, the notations and graphical representations analogous to those shown in **Fig. 3.6**, **3.7** were used.

As a result of the performed calculations, the characteristic velocities of the combustion products were determined, amounting to $\tilde{V} = 618.5$ m/s and V = 750 m/s. A comparison of the obtained values with the previously calculated corresponding values for fresh propellant showed that the difference between them does not exceed 2.5–3.5%, which indicates the preservation of the overall gas-dynamic characteristics of the process and confirms the correctness of the adopted computational model.

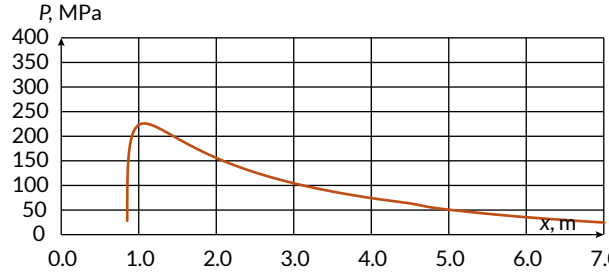

Fig. 3.8 Results of the calculation of the change in the propellant gas pressure for a reduced charge when its energy capacity is decreased by 8% in the space behind the projectile
*Source: data from the **Tables 3.2**, **3.3***

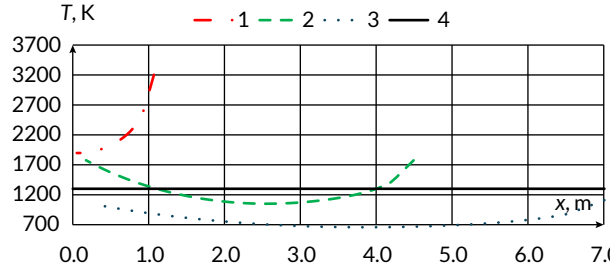

Fig. 3.9 Results of the calculation of changes in the propellant gas temperature for a reduced propellant charge when its energy capacity is decreased by 8%. Distribution of the propellant gas temperature at various projectile positions: 1 – at the moment of maximum pressure in the space behind the projectile; 2 – at the end of propellant charge combustion; 3 – when the projectile is located at the muzzle; 4 – temperature boundary of the Boudouard-Bell reaction
*Source: data from the **Tables 3.2**, **3.3***

The pattern of changes in the pressure and temperature profiles of the combustion products generally remained similar to those shown in **Fig. 3.6**, **3.7**. At the same time, the absolute values of these parameters underwent significant changes. In particular, in the considered case, the expected decrease in maximum pressure is observed. Simultaneously, the temperature levels in most of the combustion products' volume, as well as during the majority of the process duration, remain below the threshold value that determines the possibility of the Boudouard-Bell reaction occurring. This circumstance indicates a reduction in the intensity of this reaction and, consequently, an increased likelihood of the formation of a condensed phase, primarily carbon.

To assess the range of variation in the temperature of the combustion products when varying the charge amount, an additional calculation was performed for a mass of fresh propellant m = 18.4 kg, corresponding to the full charge. The results of this calculation are presented in **Fig. 3.10**, **3.11**. In their presentation, the notations and range of displayed quantities are consistent with those used in **Fig. 3.6**, **3.7**. This ensures a clear comparison and continuity in the analysis of the obtained data.

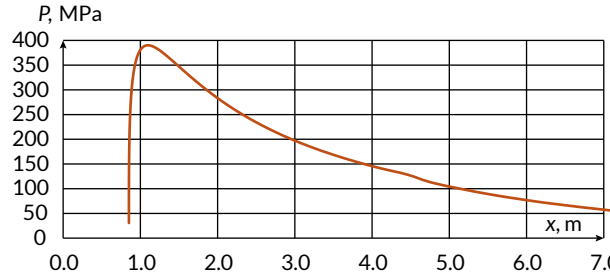

Fig. 3.10 Results of the calculation of the change in the propellant gas pressure for a full charge of fresh propellant in the space behind the projectile
*Source: data from the **Tables 3.2**, **3.3***

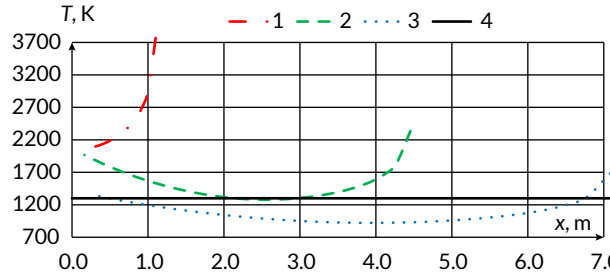

Fig. 3.11 Results of the calculation of the change in the propellant gas temperature for a full charge of fresh propellant. Distribution of the propellant gas temperature at various projectile positions: 1 – at the moment of maximum pressure in the space behind the projectile; 2 – at the end of propellant charge combustion; 3 – when the projectile is at the muzzle; 4 – the temperature boundary of the Boudouard-Bell reaction
*Source: data from the **Tables 3.2**, **3.3***

For the case under consideration, the reference values of the characteristic velocities were taken as V = 945 m/s and $\tilde{V}$ = 756 m/s. The conducted calculations yielded refined values of these parameters, amounting to V = 944 m/s and

$\tilde{V} = 780$ m/s, respectively. The practical coincidence of one of the velocities with the reference value and the moderate deviation of the other indicate satisfactory agreement of the calculated data with the initial assumptions and confirm the robustness of the chosen model for describing the process.

A characteristic feature of the obtained results is that the temperature of the combustion products near the bottom of the charge chamber, as well as in the muzzle region, exceeds the threshold value that determines the possibility of the Boudouard-Bell reaction. This circumstance is of fundamental importance for interpreting the physicochemical processes accompanying the muzzle blast. Under conditions where the temperature exceeds this threshold, the formation of a condensed carbon phase becomes thermodynamically unfavorable, and consequently, the sooty component in the combustion products does not form.

In other words, during the initial and final phases of the muzzle blast, the presence of soot in the ejected combustion products is not expected, which may have a noticeable effect both on the optical characteristics of the muzzle flame and on the overall structure of the gas outflow from the barrel.

3.4.4 What the calculation results show: determination of the ignition point and the shape of the muzzle flash

The considered model of internal ballistics processes is based on a number of fundamental assumptions that allow a significant simplification of the mathematical description of the phenomena taking place, thereby making the model suitable for performing preliminary calculations. In particular, the model employs averaged parameters of the propellant gases, simplified relations for their expansion, and idealized boundary conditions, which undoubtedly limits the strict applicability of the model. Nevertheless, a comparison of the simulation results with known experimental and computational data shows that the obtained dependencies of propellant gas pressure variations along the barrel during a shot do not contradict, either qualitatively or quantitatively, the generally accepted concepts of internal ballistics.

At the same time, an analysis of the thermal regime of the propellant gases revealed a number of features worthy of separate consideration. The nature of the temperature variation of propellant gases along the barrel during a shot proved to be considerably more complex and cannot be described by a monotonic or quasi-linear distribution. The performed calculations showed that, for a significant portion of the shot duration, the propellant gas temperature values in the initial and muzzle regions of the barrel exceed the corresponding values in its central part. Thus, the

temperature field in the barrel exhibits a pronouncedly non-uniform character, with temperature maxima localized in regions different from the geometric center of the space behind the projectile.

It should be noted that in most available sources, such a feature of the temperature distribution is either not considered or not explicitly recorded, which is likely due both to the limited capabilities of experimentally measuring the propellant gas temperature along the barrel and to the use of simpler computational models. At the same time, a similar pattern of temperature variation along the barrel can be observed, for example, in [8], which presents numerical simulation results demonstrating elevated temperature values near the beginning and end of the barrel (**Fig. 3.12**). In this figure, the horizontal axis represents coordinates along the barrel length from the breech (0) to the muzzle (7), and the vertical axis represents time during the shot. Points at the boundary between parts of the image in the upper-left and lower-right corners (light blue) indicate the position of the projectile base (horizontal axis) at the corresponding moments in time (vertical axis). The distance from any point on this boundary to the vertical axis represents, at the corresponding moment (vertical axis), the length of the barrel portion behind the projectile occupied by the propellant gases. Changes in the color scale along this segment reflect the spatial distribution of propellant gas temperatures behind the projectile at the given moment.

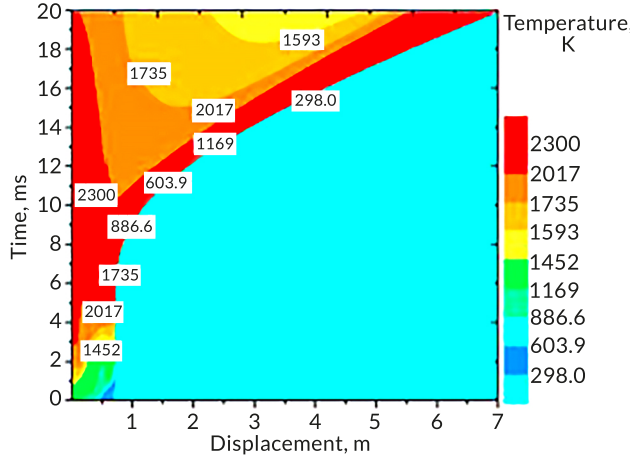

Fig. 3.12 Temperature distribution along the barrel of a large-caliber gun during a shot
Source: [8]

The results obtained in the present work, despite their approximate nature, can be considered as a theoretical basis for further analysis of the relationship between the parameters of the propellant gas expansion process in the barrel and the features of muzzle flash formation. In particular, the identified non-uniformity of the temperature field may have a significant impact on the intensity of chemical and gas-dynamic processes in the muzzle region, which opens up prospects for a more detailed study of the mechanisms of muzzle flash initiation and development based on refined internal ballistics models.

Analysis of images of the muzzle blast and the accompanying flash shows that their structure and characteristics vary significantly depending on the firing conditions. The observed diversity of spatio-temporal forms of the muzzle blast indicates the complex nature of the physicochemical processes occurring in the projectile chamber.

As a characteristic example, consider the results of muzzle blast visualization for the 2A36 gun. The images presented in **Fig. 3.1**, **3.3** clearly show that soot clouds are present along the entire length of the muzzle blast. The soot is evenly distributed along the jet, giving the blast a uniform dark appearance accompanied by intense glow during subsequent combustion.

A different picture is observed in **Fig. 3.2**. In this case, the soot-containing region occupies only part of the muzzle blast, and its volume is noticeably smaller compared to the corresponding regions in **Fig. 3.1**, **3.3**. Moreover, at least two zones with almost no soot can be distinguished in the structure of the muzzle blast in **Fig. 3.2**. The first is located at the front of the blast, ahead of the soot cloud (**Fig. 3.2**, ***b***) and is highlighted with a red contour. The second zone is behind the soot cloud, closer to the muzzle face of the barrel (**Fig. 3.2**, ***c***), and is marked with a yellow contour. It should be noted that against the bright glow of burning soot, these zones are weakly visible and become discernible only upon detailed image analysis.

One of the characteristic features of the muzzle blast is the spatial location of the muzzle flash initiation point. Analysis of the experimental data presented in **Fig. 3.1**, ***a*** and **Fig. 3.2**, ***a*** shows that in some cases, ignition of the muzzle blast is initiated at the front of the soot cloud, highlighted in red in the corresponding images. At the same time, the results shown in **Fig. 3.3**, ***b*** indicate a qualitatively different scenario: the initiation of the muzzle flash occurs in a region immediately adjacent to the muzzle face. Thus, experimental observations reveal variability in the location of the ignition zone.

These features of the muzzle blast and flash are explained by the results of approximate thermochemical calculations based on the proposed model. The data presented in **Fig. 3.7**, **3.9** indicate that by the time the projectile reaches the muzzle, temperature conditions favorable for the Boudouard-Bell reaction, accompanied by solid carbon (soot) formation, are established along almost the entire barrel length.

However, the realization of these conditions strongly depends on the state of the propellant charge.

In the case of a degraded propellant charge (**Fig. 3.9**), the temperature of the PG drops below the threshold value corresponding to the onset of carbon monoxide disproportionation even before the projectile exits the barrel. This leads to a high likelihood of soot formation throughout the projectile chamber. As a result, soot particles are present along the entire length of the muzzle blast, which is consistent with the experimental observations shown in **Fig. 3.1**, **3.3**, ***b***.

A different situation occurs when using a fresh propellant charge (**Fig. 3.7**). In this case, the PG temperature drops below the characteristic level of approximately 1300 K only in localized regions – near the chamber and at the base of the projectile – and only during the final stage of its travel through the barrel, immediately before exiting the bore. Under these conditions, the likelihood of soot formation in the initial and final phases of the muzzle blast is significantly lower than in its middle part. Such a distribution of the soot phase may correspond to the experimental picture shown in **Fig. 3.2**.

Definitive confirmation of this scenario is provided by the calculations for a full fresh propellant charge (**Fig. 3.11**). According to these data, by the time the projectile is near the muzzle, the high PG temperature in the chamber and at the base of the projectile prevents soot formation along the entire projectile chamber. Therefore, soot inclusions in the muzzle blast occupy only a limited section of its length, which also agrees with experimental observations (**Fig. 3.2**).

The spatial location of the muzzle flash initiation point can be further explained by considering the PG temperature profile along the barrel. Calculations show the presence of temperature maxima in the chamber region and near the muzzle face. The ignition temperatures of the main combustible components of the muzzle blast – hydrogen (around 800 K) and carbon monoxide (around 900 K) – play a significant role. As follows from the calculation data (**Fig. 3.6**–**3.8**), during PG expansion and outflow, their temperature can fall below these limits, and this decrease continues even after the gases exit the barrel.

As a result, under certain combinations of firing parameters, propellant charge state, and thermodynamic outflow conditions, ignition of the combustible components of the muzzle blast may not occur. In such cases, a muzzle flash does not form, as observed in **Fig. 3.13**.

Thus, the presence, spatial localization, and intensity of the muzzle flash are determined by the combined influence of the temperature field of the propellant gases, the kinetics of soot formation, and the ignition conditions of the gas phase outside the bore.

a *b*

Fig. 3.13 Stages of muzzle blast development of a 155 mm M109 (Paladin) self-propelled howitzer round. No muzzle flash occurred. Yuma Test Range: *a* – developed muzzle blast cloud with pronounced lateral lobes observed in the absence of visible ignition; *b* – further expansion and rarefaction of the discharge cloud without flame formation
Source: [17]

The examples presented above clearly demonstrate the complex, multivalued, and nonlinear relationship between the parameters of the internal ballistic processes of a shot and its external manifestations, in particular the characteristics of the muzzle outflow and the muzzle flash. The formation of these external effects is governed by the combined action of thermo-gas-dynamic processes within the bore, the evolution of propellant-gas pressure, the burning rate of the charge, as well as the conditions of combustion-product discharge beyond the muzzle. Even minor variations in internal parameters may lead to qualitatively different external manifestations, which substantially complicates the direct interpretation of observed effects.

At the same time, the parameters of internal ballistics are not invariant and depend to a large extent on the current condition of the elements of the artillery system. Among the determining factors, first and foremost, are the condition of the propellant charge and the technical state of the barrel. The degree of propellant-charge degradation caused by aging, moisture exposure, thermal cycling, and mechanical damage leads to changes in its energetic and kinetic characteristics, including the burning rate, heat of explosion, and gas generation. Similarly, wear of the bore – manifested as an increase in diameter, distortion of rifling geometry, and changes in surface roughness – has a noticeable effect on projectile motion conditions, propellant-gas leakage, and the pressure distribution along the barrel.

The combined influence of these factors results in internal ballistic parameters effectively carrying information about the current technical condition of the artillery system. Consequently, given an adequate physico-mathematical model

describing the relationship between internal processes and the external manifestations of a shot, it becomes fundamentally possible to develop a method for diagnosing the system state directly during firing and in real time.

The proposed model makes it possible to treat this problem as an inverse problem of internal ballistics, in which the internal parameters of the system – including the degree of barrel wear and the degree of propellant-charge degradation – must be reconstructed from measured or recorded external indicators of the shot (parameters of the muzzle outflow, the intensity and shape of the muzzle flash, and the temporal characteristics of gas discharge).

It should be noted that solving inverse problems of internal ballistics is associated with significant computational difficulties. These arise from the nonlinearity of the governing equations, their stiffness, and the non-uniqueness of the correspondence between internal parameters and observable external effects. Direct numerical solution of such a problem in real time is generally difficult or practically impossible when using standard computational approaches.

To overcome these limitations and to enable the operational use of results during firing, it is expedient to apply the so-called "library" method [13]. The essence of this method lies in the preliminary formation of an extensive array (library) of solutions to the direct internal ballistics problem for various combinations of system state parameters. Each element of the library corresponds to a set of characteristics of the external manifestations of a shot, calculated or obtained experimentally for a fixed state of the artillery system.

Within the framework of the problem under consideration, the library can be formed by recording the parameters of the muzzle outflow and muzzle flash for known and fixed values of barrel wear and propellant-charge degradation. During actual firing, the measured external parameters are compared with the library entries, which makes it possible to estimate the current state of the system with acceptable accuracy and minimal computational cost. This approach provides a compromise between the physical fidelity of the model and the requirements for computational efficiency, making it promising for practical implementation in technical monitoring systems and automated control of artillery complexes.

Conflict of interest

The authors declare that they have no conflict of interest in relation to this research, whether financial, personal, authorship or otherwise, that could affect the research and its results presented in this paper.

Use of artificial intelligence statement

The authors declare that they did not use artificial intelligence tools in preparing this manuscript.

Authors' contributions

Oleksandr Brunetkin: Conceptualization, Methodology, Theoretical framework, Thermochemical analysis, Mathematical modeling, Writing – original draft.

Volodymyr Demydenko: Numerical simulation, Data analysis, Model validation, Visualization.

Yevhenii Dobrynin: Experimental data interpretation, Image analysis of muzzle phenomena, Formal analysis.

Pavlo Gultsov: Literature review, Data curation, Comparative analysis, Writing – review & editing.

Oleksandr Sidelnykov: Interpretation of results, Validation, Writing – review & editing.

References

1. Brunetkin, O., Maksymov, M., Brunetkin, V., Maksymov, O., Dobrynin, Y., Kuzmenko, V., Gultsov, P. (2021). Development of the model and the method for determining the influence of the temperature of gunpowder gases in the gun barrel for explaining visualize of free carbon at shot. Eastern-European Journal of Enterprise Technologies, 4 (1 (112)), 41–53. https://doi.org/10.15587/1729-4061.2021.239150
2. Jensen, T. L., Moxnes, J. F., Unneberg, E., Dullum, O. (2014). Calculation of Decomposition Products from Components of Gunpowder by using ReaxFF Reactive Force Field Molecular Dynamics and Thermodynamic Calculations of Equilibrium Composition. Propellants, Explosives, Pyrotechnics, 39 (6), 830–837. https://doi.org/10.1002/prep.201300198
3. Pantea, D., Brochu, S., Thiboutot, S., Ampleman, G., Scholz, G. (2006). A morphological investigation of soot produced by the detonation of munitions. Chemosphere, 65 (5), 821–831. https://doi.org/10.1016/j.chemosphere.2006.03.027
4. Podlesak, D. W., Huber, R. C., Amato, R. S., Dattelbaum, D. M., Firestone, M. A., Gustavsen, R. L. et al. (2017). Characterization of detonation soot produced

during steady and overdriven conditions for three high explosive formulations. AIP Conference Proceedings, 1793, 030006. https://doi.org/10.1063/1.4971464
5. Yan, C., Zhu, C. (2023). Quantitative assessment method of muzzle flash and smoke at high noise level on field environment. Scientific Reports, 13 (1). https://doi.org/10.1038/s41598-023-27722-0
6. Muthurajan, H., Ghee, H. (2008). Software Development for the Detonation Product Analysis of High Energetic Materials – Part I. Central European Journal of Energetic Materials, 5 (3–4), 19–35. Available at: https://www.researchgate.net/publication/228786423_Software_Development_for_the_Detonation_Product_Analysis_of_High_Energetic_Materials-Part_I
7. Li, P., Zhang, X. (2021). Numerical research on adverse effect of muzzle flow formed by muzzle brake considering secondary combustion. Defence Technology, 17 (4), 1178–1189. https://doi.org/10.1016/j.dt.2020.06.019
8. Rashad, M., Zhang, X., El Sadek, H. (2014). Interior Ballistic Two-Phase Flow Model of Guided-Projectile Gun System Utilizing Stick Propellant Charge. Propellants, Explosives, Pyrotechnics, 39. https://doi.org/10.1002/prep.201400034
9. Otón-Martínez, R. A., Velasco, F. J. S., Nicolás-Pérez, F., García-Cascales, J. R., Mur-Sanz de Galdeano, R. (2021). Three-Dimensional Numerical Modeling of Internal Ballistics for Solid Propellant Combinations. Mathematics, 9 (21), 2714. https://doi.org/10.3390/math9212714
10. Kozlov, O., Maksymov, O., Maksymov, M., Riaboshapka, R. (2025). Fuzzy Control Model with Automated Rule Base Generation for Artillery Systems in Game Simulators. Energy Engineering and Control Systems, 11 (2), 157–168. https://doi.org/10.23939/jeecs2025.02.157
11. Paraschiv, T., Tiganescu, T. V., Iorga, G. O., Ginghina, R. E., Grigoroiu, O. C. (2020). Experimental and Theoretical Study on Three Combustion Models for the Determination of the Performance Parameters of Nitrocellulose – Based Propellants. Revista de Chimie, 71 (9), 87–97. https://doi.org/10.37358/rc.20.9.8320
12. Brunetkin, O., Maksymov, M., Dobrynin, Y., Demydenko, V., Sidelnykov, O. (2024). Development of a process model for determining the composition and energy characteristics of a pyrotechnic mixture using the library method. EUREKA: Physics and Engineering, 5, 99–112. https://doi.org/10.21303/2461-4262.2024.003453
13. Brunetkin, O., Davydov, V., Butenko, O., Lysiuk, G., Bondarenko, A. (2019). Determining the composition of burned gas using the method of constraints as a problem of model interpretation. Eastern-European Journal of Enterprise Technologies, 3 (6 (99)), 22–30. https://doi.org/10.15587/1729-4061.2019.169219

14. Anipko, O. B., Khaykov, V. L. (2012). Methods analysis for assessment of propellant charges as a part of the artillery ammunition monitoring system. Integrirovannye tekhnologii i energosberezhenie, 3, 60–71. Available at: http://repository.kpi.kharkov.ua/handle/KhPI-Press/2199
15. Brunetkin, O., Maksymov, M. V., Maksymenko, A., Maksymov, M. M. (2019). Development of the unified model for identification of composition of products from incineration, gasification, and slow pyrolysis. Eastern-European Journal of Enterprise Technologies, 4 (6 (100)), 25–31. https://doi.org/10.15587/1729-4061.2019.176422
16. Rusyak, I. G., Tenenev, V. A. (2020). Modeling of ballistics of an artillery shot taking into account the spatial distribution of parameters and backpressure. Computer Research and Modeling, 12 (5), 1123–1147. https://doi.org/10.20537/2076-7633-2020-12-5-1123-1147
17. Official U. S. Army Twitter. Available at: https://x.com/USArmy